Cellulose (2024) 31:1533–1544
https://doi.org/10.1007/s10570-023-05714-7

ORIGINAL RESEARCH

Retain strength, gain ductility: tough and transparent nanopapers by mercerisation

Florian Mayer · Alexander Prado-Roller · Andreas Mautner · Alexander Bismarck

Received: 30 June 2023 / Accepted: 22 December 2023 / Published online: 4 January 2024

Abstract Nanocellulose papers offer high tensile strength and modulus but suffer from drawbacks such as their brittle nature. We show that mercerisation of cellulose nanopapers in strong alkaline media for 2 min to 24 h results in the (partial) transformation of native cellulose I into the more ductile cellulose II allomorph. The strain to failure of mercerised nanopapers tripled compared to the original nanopapers while retaining their tensile strength in excess of 100 MPa at the expense of a slight drop in modulus resulting in a significant increase in toughness (total work of fracture). An additional advantage of mercerisation is a reduction in porosity of the nanopapers and increased transparency.

Keywords Nanocellulose · Mercerisation · Nanopapers · All cellulose composites · Toughness

Introduction

Thin nanocellulose films, also called nanopapers, show great potential in a myriad of possible applications such as substrates for printable electronics (Koga et al. 2013, 2014; Fujisaki et al. 2014; Zhu et al. 2014), water treatment membranes (Mautner et al. 2015, 2016, 2019; Mautner 2020; Fijoł et al. 2023), and as 2 dimensional reinforcement for

Supplementary Information The online version contains supplementary material available at https://doi.org/10.1007/s10570-023-05714-7.

F. Mayer · A. Mautner · A. Bismarck
Institute of Materials Chemistry and Research, Polymer and Composite Engineering (PaCE) Group, Faculty of Chemistry, University of Vienna, Währinger Straße 42, 1090 Vienna, Austria

A. Prado-Roller
Institute of Inorganic Chemistry - Functional Materials, Faculty of Chemistry, University of Vienna, Währinger Straße 42, 1090 Vienna, Austria

A. Mautner (✉)
Institute of Environmental Biotechnology, IFA-Tulln, University of Natural Resources and Life Sciences, Vienna, Konrad-Lorenz-Straße 20, 3430 Tulln an der Donau, Austria
e-mail: andreas.mautner@boku.ac.at

A. Bismarck
Department of Chemical Engineering, Imperial College London, South Kensington Campus, London SW7 2AZ, UK

A. Bismarck (✉)
Division of Materials Science, Department of Engineering Sciences and Mathematics, Luleå University of Technology, Luleå 971 87, Sweden
e-mail: alexander.bismarck@univie.ac.at

polymers (Mautner et al. 2017, 2020) amongst many others. These applications pose different requirements on nanopapers, rendering the tuneability of the mechanical, optical and morphological properties a necessity. Specifically, nanopapers prepared from cellulose nanofibrils (CNFs) by filtration and hot-pressing akin to traditional papermaking are promising for these applications. Such cellulose nanopapers are stiff and strong but brittle (Hervy et al. 2017), lack full transparency (Xu et al. 2016), and are sensitive to moisture resulting in low wet strength (Kriechbaum and Bergström 2020; Walther et al. 2020). A variety of methods to address this conundrum have been reported. For instance, we suggested a hybridisation approach to fashion nanopapers with improved tensile strength, strain to failure and toughness by hybridising different types of nanofibrils exhibiting various dimensions and exploiting their different chemical and mechanical properties (Mautner et al. 2018). Sehaqui et al. (2011) dried unmodified and TEMPO-oxidised nanocellulose using supercritical CO_2 to prepare nanopapers with high strain to failure while Guzman-Puyol et al. (2022b) prepared papers from C6 fluorinated nanocellulose esters to considerably increase the toughness of the resulting nanopapers. The same group (Guzman-Puyol et al. 2022a) also reported a method to combine nanocellulose and naringin in trifluoroacetic acid and cast films from these mixtures, which exhibited increased toughness and UV-blocking capabilities. Kriechbaum and Bergström (2020) produced optically transparent nanocellulose films with high wet strength and UV-blocking properties by grafting nanocellulose with gelatin moieties followed by impregnation of films prepared from this material with a gelatin and tannin solution, which resulted in films with greatly improved wet strength while sacrificing strain to failure and toughness in the dry state. Gindl and Keckes (2005) and Abbott and Bismarck (2010) prepared all-cellulose composites by first solvent exchanging nanocellulose to dimethylacetamide and subsequently partially dissolving the nanofibrils using LiCl/dimethylacetamide followed by regeneration to all-cellulose composites with high tensile strength and optical transparency. All the processes detailed above are either time-consuming and/or resource-intensive chemical procedures to modify the raw material or employ expensive reagents, additives or treatment methods. To tailor strength and stiffness without sacrificing toughness (or work of fracture) methods need to be developed that could be easily implemented into existing industrial processes adding little extra cost to be viable for broad industrial applications.

Auspiciously, cellulose itself offers a solution to this problem as it can be transformed into different allomorphs covering a broad array of mechanical properties. The naturally occurring cellulose allomorph (cellulose I) is synthesised by plants, bacteria and some animals. Cellulose II does not occur in nature and, thus, is often referred to as "synthetic cellulose". Cellulose I exhibits a more ordered structure, with its crystalline regions being formed by layers of parallel cellulose molecules formed via hydrogen bonds stacked on top of each other and held together through hydrophobic interactions (Nishiyama et al. 2002, 2003). Cellulose II on the other hand is composed of a tight 3D network of hydrogen bonded cellulose molecules with some disorder in the pattern (Kroon-Batenburg and Kroon 1997). The differences in structure between cellulose I and II also affect their mechanical properties: Cellulose I has a Young's modulus and ultimate tensile strength approximately 50% higher than that of cellulose II according to modelling reports (Nishino et al. 1995; Moon et al. 2011; Djahedi et al. 2015). Cellulose I can be transformed into cellulose II using a simple yet efficient alkaline treatment, commonly referred to as mercerisation named after John Mercer, a British scientist who invented the process in 1844 (Binz 1898). Mercerisation is widely used in the textile industry to improve the lustre and sheen of cotton fibres. This transformation is hypothesised to occur by swelling individual cellulose elementary fibrils, which constitute the macroscopic cotton fibres, causing neighbouring fibres to interdigitate and thus transforming cellulose I into cellulose II (Kim et al. 2006). The thermodynamically more stable cellulose II is more ductile compared to cellulose I (Gindl and Keckes 2005).

Alkaline treatment was already applied to nanocellulose, but to date, it was almost exclusively performed directly on nanocellulose suspensions, e.g. as a purification step to remove organic residues from bacterial cellulose cultures, i.e. nanocellulose synthesised by various strains of bacteria, such as *Komatagaeibacter*, or to degrade and solubilise hemicellulose residues from wood pulp derived nanocellulose. Mercerisation is hypothesised to require the interdigitation of two antiparallel

aligned nanocellulose (Kim et al. 2006) fibrils that are right next to each other, alkaline treatment of individualised fibrils in suspension usually does not result in the transformation of cellulose I fibrils into the cellulose II as they are well separated in suspension and thus the interdigitation step of the process is impeded. To produce cellulose II nanofibres with significantly higher toughness yet lower ultimate tensile strength in nanopaper form as compared with standard CNF nanopapers, Wang et al. (2014) combined mercerisation of wood pulp with extensive sodium chlorite treatment prior to defibrillation in a homogeniser. Faria-Tischer et al. (2015) used an alkaline treatment to fully convert as-grown bacterial cellulose pellicles into cellulose II and reported improved transparency and smoother surfaces of the resulting compacted mercerised pellicles. Hu et al. (2022) mercerised never dried, as-grown bacterial cellulose tubes to produce small-calibre vascular grafts with enhanced mechanical properties. Wloch et al. (2023) used alkaline treatment on never dried, as-grown bacterial cellulose pellicles and found that mercerized pellicles had significantly higher strains to failure but lost up to 40% in tensile strength. Mercerised BC pellicles were also used to fabricate low cellulose loading optically transparent composites. Mercerisation of ready-made, dried and 'hornified' CNF nanopapers to improve their tensile and optical properties has not been reported before but could be a simple, low-cost method to obtain nanopapers with tailored mechanical properties.

We propose that alkaline treatment of a randomly oriented and compacted network of nanocellulose fibrils will result in effective partial mercerisation of the whole nanopaper sheet. We hypothesise that the outer layers of individual nanofibrils in contact with other fibrils can be (partially) transformed into cellulose II resulting in an all-cellulose composite comprising a cellulose I core embedded in a matrix of weaker yet more ductile cellulose II. This process is anticipated to also increase the optical transparency of the nanopapers as both swelling and interdigitation should reduce the porosity and thus the haze of the nanopapers, increasing their suitability, e.g. for composites, packaging materials or surface coatings. Particular focus is placed on the use of nanocellulose produced in a simple and cost-effective way without prior enzymatic or chemical treatments or classification processes.

Experimental

Materials

Sodium hydroxide pellets were purchased from W. Neuber's Enkel (Vienna, Austria). We produced CNFs from never-dried elemental chlorine-free bleached softwood (*Picea abies and Pinus spp.*) pulp, obtained from Stendal (Berlin, Germany). The pulp comprised 81.3% cellulose, 12.6% hemicellulose and 0.3% ash (Josset et al. 2014). Unless specified otherwise, deionised water was used in all experiments.

Preparation of nanocellulose

Nanocellulose was prepared by cutting 100 g of pulp into small pieces (approx. 10×10 mm^2) and submerging them for 18 h in 1 L of water prior to blending (Kult Pro, WMF, Germany) at 1200 W for 1 min. The resulting homogeneous suspension was then passed 10 times through a high-speed disc mill (Granomat JP 150, Fuchs, Switzerland). The ten-step gap size indicator of the grinder was set to 10, marking the distance at which two grindstones just touched resulting in an audible sound. After the addition of the cellulose suspension the gap size was continuously reduced, starting at 9 during the first pass down to 5.5 during the tenth cycle. More water was added after each pass as required to ensure a consistency suitable for passing the dispersion through the mill. In lieu of specific measurements, and because of the constantly changing state of the suspension due to fibre defibrillation, and thus the gradual increase of the viscosity of the suspension, water was added to keep the viscosity somewhere between that of whole milk (2 mPa s) and Ketchup (2000 mPa s) (Koocheki et al. 2009). The resulting nanocellulose suspension was up-concentrated to 4 wt% by gravity filtration through a cotton cloth and then stored at 4 °C until use.

Preparation of nanocellulose papers

Papers with a grammage of 50 g m^{-2} were prepared by blending nanocellulose (0.613 g dry weight) with water in a kitchen blender (Kult Pro, WMF, Germany) at 1200 W for 30 s to obtain a homogeneous CNF suspension with a consistency of 0.2 wt%. This suspension was then vacuum filtered using a Büchner funnel with a 125 mm diameter fritted glass disc onto

a filter paper (VWR 413, VWR, Leuven, Belgium) to obtain a filter cake, which was subsequently sandwiched between 4 sheets of blotting paper (3MM Chr VWR, Lutterworth, UK) and pressed in a hydraulic press (type 25-12-2 H, Carver Inc., Wabash, USA) at 20 °C for 10 s under a weight of 1.5 ton-force to remove excess water. The pre-pressed filter cake was then sandwiched between steel plates, fresh blotting and release paper and hot pressed at 120 °C for 15 min under 1.5 ton-force to consolidate the nanopapers.

Mercerisation of nanocellulose papers

Nanopapers were framed in a custom-made PMMA frame (Fig. 1) consisting of two identical rings with an inner diameter of 100 mm and an outer diameter of 150 mm, which was laser-cut from 3 mm thick PMMA sheets and fixed with eight M8 stainless steel bolts each tightened with a torque wrench set to 5 Nm to apply even pressure across the outside of the nanopapers preventing shrinkage that commonly occurs during mercerisation (Goldthwait 1965). This frame system, holding a nanopaper, was subsequently immersed into NaOH solutions of various concentrations for defined time intervals (Table 1).

After treatment, the frame holding the mercerised paper was removed from the alkaline bath and rinsed with tap water (approx. 10 L) until pH 7 removing NaOH. Afterwards, the papers were removed from the PMMA frame, sandwiched between four sheets of blotting paper (two on top, two on bottom) and dried at 110 °C for 24 h between two stainless steel plates under 10 kg-force to avoid warpage.

Table 1 Preparation parameters and names of all samples. Samples were prepared in duplicates

Sample name	NaOH concentration		Treatment time
	wt%	[mol L^{-1}]	[min]
Ref	0	0	0
20% 2 min	20	6.1	2
20% 10 min	20	6.1	10
20% 60 min	20	6.1	60
20% 24 h	20	6.1	1440
40% 2 min	40	14.3	2
40% 10 min	40	14.3	10
40% 60 min	40	14.3	60

Chemical composition determined by X-ray photoelectron spectroscopy

The surface composition of nanopapers before and after mercerisation was analysed by X-ray photoelectron spectroscopy (XPS). For each sample, a survey spectrum with a step size of 1 eV and a pass energy of 200 eV was recorded. Element-specific high-resolution spectra for carbon (C1s 279–298 eV), nitrogen (N1s 392–410 eV), oxygen (O1s 525–545 eV), as well as sodium (Na1s 1062–1079 eV), calcium (Ca2p 340–360) and silicon (Si1p 95–110 eV) with step sizes of 0.1 eV and a pass energy of 50 eV, were acquired. All spectra were recorded using Al-K_α X-rays at 72 W at a spot size of 400 µm on a photoelectron spectrometer (Nexsa, Thermo Scientific, UK). After the initial measurement, the sample surfaces were ablated using a beam of Ar clusters of 1000 atoms and an energy of 6 keV. Peak fitting

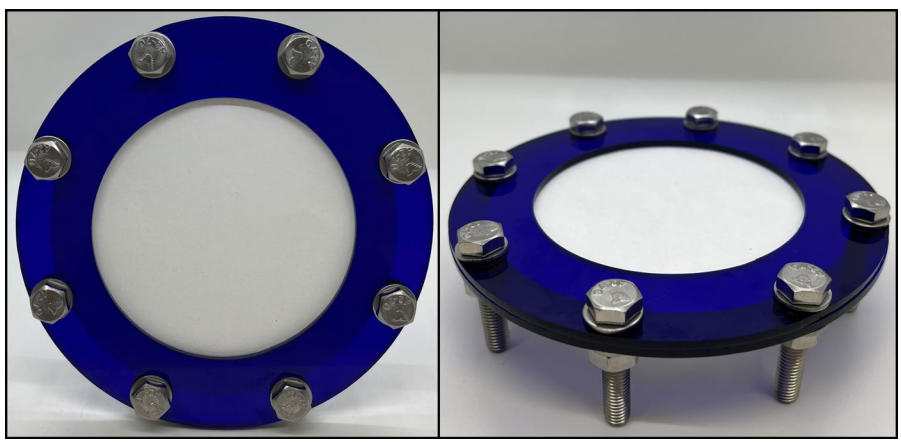

Fig. 1 Front and side view of the custom-made PMMA frame used during mercerisation to ensure the dimensional stability of nanopapers during treatment

was performed using the software package Avantage (v5.9931, Thermo Fisher Scientific, UK) and the atomic composition was calculated from the peak area using the integrated ALTHERMO1 scaling factor database.

Cellulose crystallinity determined wide-angle Powder X-ray diffraction

Wide angle powder X-ray diffraction (PXRD) was performed on cellulose films using an Empyrean Powder Diffractometer (Malvern PANalytical, Amelo, The Netherlands) using Cu-K_α X-ray source with a wavelength of 1.54 Å in θ/θ-mode. Specimens were fixed to a reflection-transmission spinner and recorded in reflection mode, using a Bragg-Brentano mirror. All measurements are continuous scans in the 2θ range of 6 to 45°, with a step size of 0.0131°, a counting time per step of 49.47 s and a spinning rotation time of 8 s. The degree of crystallinity and the crystalline composition of the cellulose samples was determined by Rietveld refinement using the ideal diffraction patterns of cellulose Iβ and II as reported by Nishiyama et al. (2002) and French (2014) using the software package High Score Plus, Version 4.9a (4.9.1.29739) (PANanalytical). A detailed description of the workflow, cif files used and Rietveld refined diffractograms can be found in SI Sect. 1.

Porosity, density and thickness of nanopapers

Eight test specimens radially distributed across one half of the paper (Fig. SI 2–1) were punched out from the mercerised and non-mercerised papers using a punch die (Zwick ZCP 020 Manual Cutting Press, Zwick, Ulm, Germany). The dogbone-shaped test specimens (EN ISO 527-2, Type 1BB) had an overall length of 30 mm with a 20 mm long and 2 mm wide middle section. The test specimens had an area A of 85.81 mm^2. The thickness d of each test specimen was measured at five points evenly distributed along their length (Fig. SI 2–1) using a digital micrometre (705-12229, RS Components, Corby, UK). The specimens were weighed using an microbalance (MSA 225P, Sartorius, Göttingen, Germany) and used to determine the average paper grammage Γ (Eq. 1), envelope density ρ_e (Eq. 2) and porosity Φ (Eq. 3) from the measured mass m, A and d of the specimens by approximating the skeletal density ρ_s of both cellulose I and II to be 1606 kg m^{-3} (Daicho et al. 2022).

$$\Gamma = \frac{m}{A} \tag{1}$$

$$\rho_e = \frac{\Gamma}{d} \tag{2}$$

$$\Phi = \frac{\rho_e}{\rho_s} \times 100 \tag{3}$$

Tensile properties of (mercerised) nanopapers

Tensile tests were performed on a minimum of at least eight specimens for each (mercerised) nanopaper sample at 25 °C and 35–40% RH using a dual column universal test frame (Instron Model 5969 Dual column Universal Testing System, Instron, Darmstadt, Germany) equipped with a 1 kN load cell. The tensile strain was recorded using a non-contact video extensometer (Gig ProE, iMETRIUM, Bristol UK). The sample thickness was approximately 50 µm. Tensile tests were performed at a gauge length of 15 mm and a crosshead displacement speed of 1 mm min^{-1}. The Young's modulus (elastic Modulus E) was determined in the linear elastic region of the stress-strain curves as a secant between two strength values separated by 0.2% strain according to a procedure previously established by us (Mautner et al. 2018). The absorbed energy during tensile fracture (J m^{-3}) was determined from the area under the stress-strain curves.

Scanning electron microscopy

To investigate the microstructure of the nanopapers before and after mercerisation, micrographs were taken using a scanning electron microscope (SEM, ZEISS Supra 55 VP, Carl Zeiss GmbH, Jena, Germany) operated at an accelerating voltage of 2 kV and a working distance of 7.2 mm. The specimens were mounted onto aluminium sample holders using carbon tape and gold coated (Leica SCD 050/EM QSG 100) at 60 mA for 60 s prior to SEM imaging.

Results and discussion

Mercerisation was primarily performed at a NaOH concentration of 20 wt% –the common concentration used for mercerisation of cellulose fibres– in accordance with previous reports (Kolpak et al. 1978; Wang et al. 2014; Faria-Tischer et al. 2015; Hu et al. 2022; Sawada et al. 2022). In addition, a concentration of 40 wt% NaOH was chosen to investigate whether harsher and more concentrated alkaline conditions would have a favourable effect on the treatment. Preliminary experiments showed that mercerisation and subsequent drying resulted in significant shrinkage and subsequent cockling of the nanopapers as the cellulose fibril network consolidated (Fig. SI 3–1). To counteract shrinkage we fixed nanopapers in a frame allowing to preserve the original dimensions of the papers as confirmed by the thickness and of the mercerised nanopapers (Table SI 3–1). All samples treated while being fixed in the frame exhibited thicknesses close to those of the samples before mercerisation with an average deviation of a mere 4%. Mercerisation of an unframed nanopaper caused swelling as the whole network contracted resulting in a thickness increase of ~20%. After mercerisation of constrained nanopapers, the envelope density of all networks increased on average by 8% corresponding to an average porosity of 32 ± 1% compared with 37 ± 2% for nanopapers prior to mercerisation.

Figure 2 juxtaposes a reference nanopaper (left) and a nanopaper mercerised in 40 wt% NaOH for 10 min (right) taken at different distances away from the original (picture of a flower). The comparative photographs show the effect of alkaline treatment on both transparency and haze, with the former increasing and the latter decreasing. These changes were primarily attributed to the reduction of porosity as well as a decrease in surface roughness of mercerised nanopapers reducing light scattering. Decreasing surface roughness after mercerisation of nanopapers was also found by Faria-Tischer et al. (2015) for mercerised bacterial cellulose nanopapers. On a macroscopic level, a smoother and more uniform surface was generated, which affected their haptic properties that changed drastically from a rough "papery" texture to a smooth, almost plastic film-like texture.

Scanning electron micrographs (Fig. 3) revealed a change of surface morphology accompanying the (partial) transformation of cellulose I to II. SEM

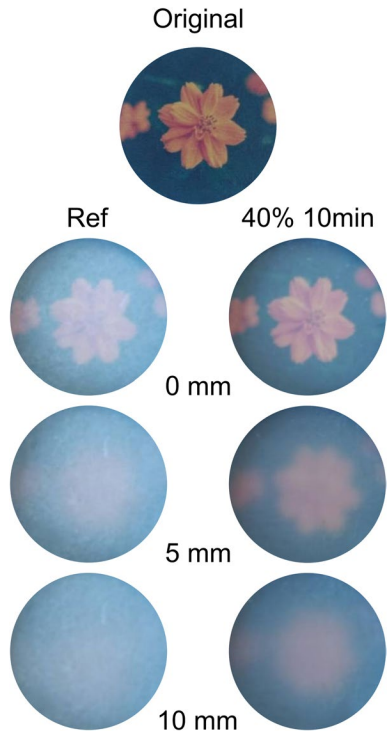

Fig. 2 Representative images of a picture of a flower (top) and of the same picture photographed through nanopapers (camera settings: shutter speed of 1/5, ISO of 80, white balance of 3200 K at fixed at a distance of 13.5 cm from reference image) before (left) and after mercerisation for 10 min in 40 wt% NaOH solution (right) directly on top of an image (0 mm) and gradually further away (5 & 10 mm, respectively)

images of the reference sample (Fig. 3A) show a fibrous network structure with distinctly visible fibrils whereas the mercerised samples showed a much less fibrillar structure on their surface (Fig. 3B–E) and fracture surfaces (Fig. SI 3–2). It appears that fibrils fused into larger fibrillar structures, which disappear with longer treatment times indicating that swelling and transformation occur gradually. Our observation is in good agreement with the postulated mechanism of mercerisation by fibre swelling and interdigitation (Kim et al. 2006).

SEM also revealed the appearance of bulbous structures on the surface of mercerised nanopapers. The amount and size of these structures increased with longer treatment times and in harsher alkaline treatment conditions. We hypothesise that the structures consist of cellulose II expulsed from the network and consequently "squeezed" through the pores

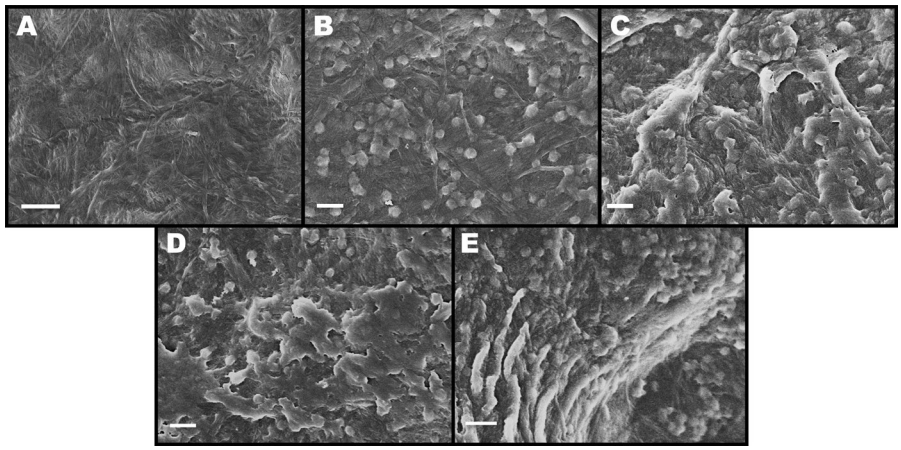

Fig. 3 SEM images of the surfaces of samples treated in 20 wt% NaOH solutions. **A** Reference, **B** 2 min, **C** 10 min, **D** 1 h, **E** 24 h. The scale bar size corresponds to 1 µm

in the surface of the network during the swelling step. A possible explanation for this rather unexpected texturing of the nanopaper surface will be attempted further below.

XPS showed that the chemical composition of the nanopapers did not change during mercerisation (Fig. SI 4–1). Un/mercerised nanopapers consisted of pure cellulose containing minute amounts of inorganic contaminants stemming from the processing of the pulp as well as from the grindstone (Fig. SI 4–2).

Wide-angle PXRD was used to monitor the transformation of cellulose I into cellulose II. Diffractograms of mercerised nanopapers (Fig. 4 and Fig. SI 1–1 to SI 1–8) show the typical diffraction peaks of cellulose I_β. We assigned the diffraction peak at $2\theta \approx 22.5°$ to the (2 0 0) diffraction plane of cellulose I_β, while the diffraction peak centred around $2\theta \approx 15.7°$ was assigned to be a compound peak of the I_β(1–1 0) and the I_β(1 1 0) diffraction plane at 15° and ~16.5°, respectively (French 2014). It should be noted, that the ideal X-ray diffraction pattern of native cellulose I should consist of two diffraction peaks with equal intensity at $2\theta = 14.5°$ and 16.5° (French 2014). The main diffraction peaks of cellulose II

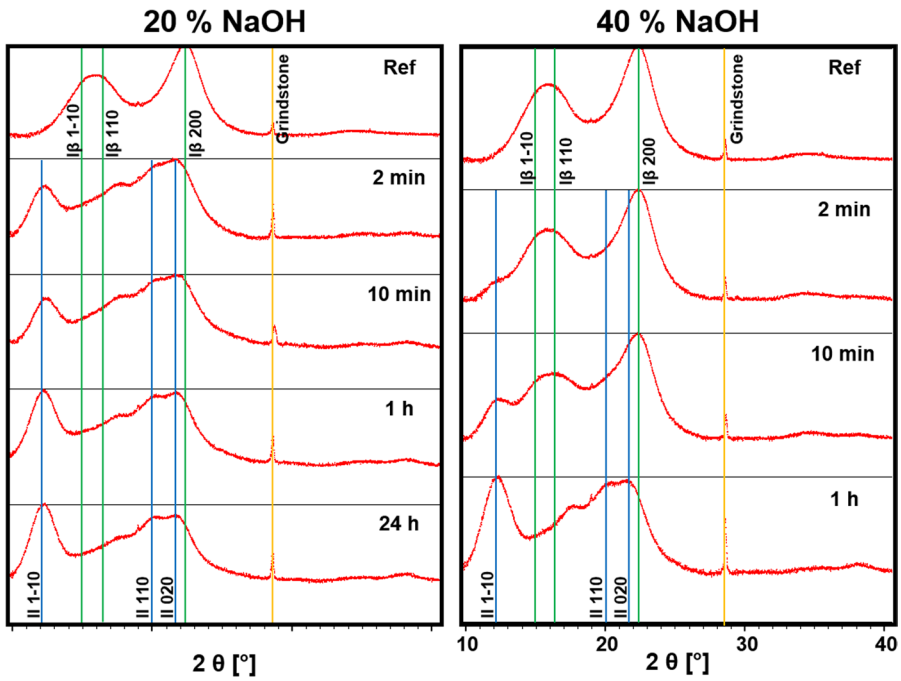

Fig. 4 Wide angle PXRD diffractograms of untreated reference papers (Ref) and nanopapers mercerised for various times in 20 wt% (left) and 40 wt% (right) NaOH concentration

occur at 2θ ≈ 12.2°, ~ 20.1° and ~ 21.7° corresponding to the (1–1 0), (1 1 0) and (0 2 0) diffraction planes of cellulose II, respectively (French 2014). The sharp diffraction peak at ~ 28.5° was attributed to presence of crystalline residue from the grindstone, which could be confirmed by the silicon found in XPS (Fig. SI 4–1 and Fig. SI 4–2).

Our starting wood-based nanocellulose possessed a degree of crystallinity of 69% in agreement with the literature (Hermans and Weidinger 1949; Ahvenainen et al. 2016; Daicho et al. 2018). During mercerisation, cellulose I_β is transformed into cellulose II as apparent in the diffractograms (Fig. 4). The overall degree of crystallinity of the cellulose did not change and remained constant at ~ 70% (Fig. 5). Samples treated with 20 wt% NaOH exhibited a rapid transformation from cellulose I to II already within the first 2 min. After a mercerisation time of 1 h, the cellulose II content increased only slightly from 59 to 61% over the course of the subsequent 23 h. The final material is still a composite comprising cellulose I crystallites embedded in a cellulose II matrix, connected by amorphous cellulose. When using 40 wt% NaOH solutions for mercerisation, the transformation from cellulose I to II occurs at a significantly lower rate resulting in a more gradual compositional change but the amorphous phase content remained constant at around 30%. We hypothesise the difference in transformation speed to be due to higher alkaline concentrations causing significantly faster swelling of the fibril surfaces, thus leading to a faster transformation of cellulose I to II slowing down access of the alkaline solution to the core regions of the fibrils—creating a "passivation" layer around a cellulose I core—resulting in an overall lower transformation rate. The XRD data thus suggest that the desired effect of obtaining a nanopaper with a core of cellulose I nanofibres fibres embedded in a matrix of cellulose II can be best achieved in 20 wt% NaOH solution at short treatment times. Treatment times in excess of 10 min result in only marginal gains of transformation to cellulose II. When using 40 wt% NaOH solutions the transition to cellulose II occurs over longer time intervals, allowing for better control of the crystalline composition.

Representative stress-strain curves of the mercerised and reference nanopapers are shown in Fig. 6. Compared to the reference sample, all mercerised samples show significantly increased strains to failure (ε_b). Nanopapers mercerised in 20 wt% NaOH solution exhibited the highest ε_b after 2 min treatment time and a subsequent decrease with increasing treatment times. Nanopapers mercerised in 40 wt%

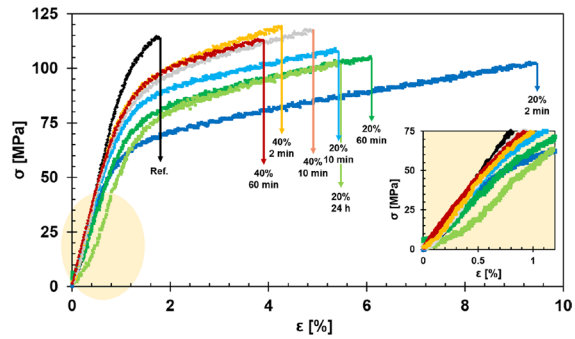

Fig. 6 Representative stress strain curves of (mercerised) nanopapers. The inset diagram shows a magnification of the linear region used to calculate E

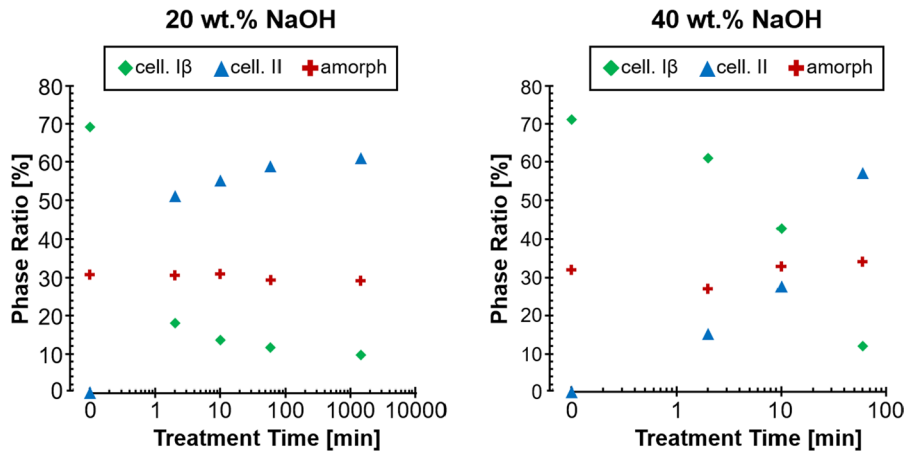

Fig. 5 Degree of crystallinity of cellulose I_β and II, as well as amorphous phase content of untreated reference papers (ref) and nanopapers mercerised for various times at 20 wt% (left) and 40 wt% (right) NaOH concentration

NaOH solutions also exhibited increased ε_b but to a lesser extent compared with the samples treated in 20 wt% alkaline solutions. The maximum ε_b of the sample subset mercerised in 40 wt% NaOH solutions was reached for a treatment time of 10 min, after which ε_b decreased again in concordance with the XRD results reported above. These suggest a slower progression of the cellulose I to II transformation in the samples mercerised in 40 wt% NaOH solution, which causes an optimal cellulose I/II ratio for the formation of an all-cellulose composite to be reached at a slower rate. The influence of the alkaline treatment on the ultimate tensile strength and strain to failure of the individual samples can be attributed to the cellulose I to II transformation occuring during mercerisation at room temperature. During alkaline pulping at elevated temperatures (e.g. at 170 ºC) cellulose molecules are hydrolysed. Longer treatment times led to cellulose with a lower degree of polymerisation (Berggren et al. 2002). However, in our case we did not observe a significant change in average molar mass between mercerised nanopaper irrespectively of mercerisation conditions (Fig. SI 5–1). The only observed change occurred in the lower molecular weight fractions, which decreased likely due to dissolution of those fractions with increasing treatment times.

Nanopapers mercerised with 20 wt% alkaline solutions had lower ultimate tensile strength compared to reference nanopapers and the values for all samples were, within their margin of error, at the same level (Table 2). Nanopapers treated in 40 wt% NaOH solution retained the ultimate tensile strength of the original nanopapers while ε_f increased. The trend found among the strain to failure, was attributed to multiple processes taking place simultaneously, however, primarily the conversion from cellulose I to the weaker and more ductile cellulose II allomorph was responsible for this effect. As the swelling and conversion process happened very fast for samples mercerised in 20 wt% solutions, no significant influence of the treatment time on their tensile strength could be detected, apart from the significantly larger margin of uncertainty for the nanopaper with 2 min treatment. The retained tensile strength of nanopapers treated for 2 and 10 min with 40 wt% NaOH was mainly attributed to the densification of the network, as observed for nanopapers that were mercerised for longer periods of time (Table SI 3−1).

Table 2 Tensile properties of mercerised nanocellulose samples containing tensile strength (σ), strain to failure (ε_f), Young's Modulus (E) and work of fracture (WoF)

Sample name	σ (MPa)	ε_f (%)	E (GPa)	WoF (MPa)
Ref	114.9 ± 2.1	1.7 ± 0.1	12.7 ± 0.9	1.2 ± 0.1
20% 2 min	102.0 ± 11.1	9.1 ± 1.3	7.2 ± 0.6	6.9 ± 1.0
20% 10 min	110.0 ± 3.2	6.0 ± 0.5	7.8 ± 0.7	5.0 ± 0.6
20% 60 min	105.4 ± 4.2	6.1 ± 1.1	7.3 ± 0.7	4.8 ± 1.1
20% 24 h	109.8 ± 6.5	5.1 ± 1.1	8.4 ± 1.2	4.1 ± 1.0
40% 2 min	118.0 ± 7.1	4.1 ± 0.7	10.6 ± 0.9	3.6 ± 0.8
40% 10 min	119.2 ± 3.3	4.6 ± 0.6	10.3 ± 0.9	4.1 ± 0.7
40% 60 min	111.7 ± 5.0	3.9 ± 0.5	9.4 ± 0.5	3.2 ± 0.5

The Young's moduli of nanopapers mercerised in 20 wt% NaOH solutions followed the inverse trend of ε_b (Table 2) and were significantly lower than those treated in 40 wt% NaOH solutions, which in turn exhibited Young's moduli lower than the reference, indicating a trade-off between stiffness and ductility. The Young's moduli and tensile strengths of mercerised nanopapers also compare well to those of cellulose II (Cellophane) films found in the literature (Fink et al. 2001; Leppänen et al. 2020). However, a direct comparison should be made with care, as those dense Cellophane membranes were prepared using different methods and starting materials were not nanofibrillated network structures and commercial cellophane films are often plasticised.

The work of fracture (WoF), i.e. the area under the stress-strain curve, which is a measure of the toughness of a material (Sehaqui et al. 2011) increases significantly for all mercerised nanopapers over that of the reference paper (1.2 MPa) following the trend for the strain to failure. A minimum increase of WoF of 175% and peak values of 6.9 MPa, corresponding to 590% of the original value, were obtained. The results of three of the nanopapers are particularly remarkable. Nanopapers mercerised for 2 min in 20 wt% NaOH exhibited the highest increase in both ε_b and WoF, while papers mercerised for 2 and 10 min in 40 wt% NaOH solution exhibited an increase both in tensile strength and strain to failure, thus significantly increasing WoF of these materials while retaining

over 80% of the Young's modulus of the original nanopaper. Our results show the beneficial effect of partial mercerisation of nanopapers forming all-cellulose composites by transformation of cellulose I to cellulose II both in terms of mechanical properties, resulting in increased toughness while retaining strength at the expense of a slight drop in modulus, and enhanced transparency. In particular, the short treatment times needed render this process suitable for a "drop-in" solution in processes where high throughput is necessary.

We investigated the mercerisation of nanopapers consisting of an in-plane randomly oriented, hornified nanocellulose I fibrillar network. We hypothesised that during mercerisation in caustic soda the fibrils in the network start swelling but in the constrained network, the swollen phase surrounding the cellulose I cores filled the pores (resulting in the reduced porosity, Table SI 3 –1) and excess near the surface was expelled through the pores (Fig. SI 6 −1). In the swollen state the transformation of celllose I to II could occur in two different places: (i) between neighbouring or intersecting fibrils thus "welding" (Wloch et al. 2023) those fibrils together and (ii) between cellulose molecules of the swollen phase extruded through the pores in the constrained fibrillar network. After regeneration this likely resulted in the bulbous structures observed on the surfaces of mercerised nanopapers (Fig. 3). The "welding" of neighbouring or intersecting fibrils possibly caused by interdigitating cellulose molecules originating from close cellulose fibrils with different cellulose I orientation created cellulose II sheaths surrounding cellulose I cores. Irrespectively of the exact mechanism of the cellulose I to II transformation during mercerisation, the results taken together with the observation that the fraction of amorphous cellulose remained unaffected by mercerisation point towards the existence of stiffer and stronger cellulose I cores embedded within the more ductile and less strong cellulose II matrix. The mechanical properties (Fig. 6) can be explained the hybridisation of cellulose I and cellulose II with a random orientation of cellulose I fibrils within the matrix. Upon loading, fibrils can reorient in the loading direction and stress is transferred through the matrix into the stiffer component. Subsequently, after raching the yield (knee) point, the stiffer cellulose I elements start failing and cellulose II takes over the stress distributing it through the material resulting in eventual final failure. The observed stress strain behaviour is in analogy to that of hybrid (Bunsell and Harris 1974) and/or angle-ply (Fuller and Wisnom 2015) composites.

Conclusion

We investigated the influence of mercerisation of pulp-derived cellulose nanopapers under pretension on their mechanical properties; two different NaOH concentrations and the effect of treatment time were investigated. Mercerisation of nanopapers causes the partial conversion of cellulose I into II resulting in significant increases of both strain to failure and toughness of the treated nanopapers as their tensile strength was retained. The transformation of cellulose I to II was confirmed by XRD. Mercerised nanopapers had a higher envelope density and thus lower porosity as compared to the original materials. We found that short mercerisation times yielded nanopapers that can be considered all cellulose composites comprising a blend of cellulose I and II offering high tensile strength, modulus and toughness. An additional benefit of mercerisation was the observed increase in transparency of the resulting nanopapers.

Acknowledgments We acknowledge funding provided by the University of Vienna through the Institute of Materials Chemistry. We are grateful to Klaus Ritter for the preliminary experiments, which in effect guided us to an improved experimental procedure. We greatly apprechiate Dr Irina Sulaeva and Prof. Antje Potthast (Department of Chemistry, Institute for Chemistry of Renewables, University of Natural Resources and Life Sciences (BOKU)) for their help in determining the cellulose molecular weight and the dicussions of the results.

Author contributions Conceptualisation of this study and experiment design by FM, AM and AB. Material preparation, data collection by FM and AP-R. Data analysis by FM, AP-R and AB. The first manuscript draft was written by FM and all authors contributed to editing the manuscript. All authors have read and approved of the final manuscript.

Funding Open access funding provided by University of Vienna. Partial financial support was received from the University of Vienna and the Institute of Materials Chemistry under Grant Number 371300.

Data Availability The corresponding author will provide raw data upon request.

Declarations

Conflict of interests The authors have no relevant financial or non-financial interests to disclose.

Ethical approval and consent to participate No ethics approval was required for this study.

Consent for publication All authors consent to the publication of this manuscript.

References

Abbott A, Bismarck A (2010) Self-reinforced cellulose nanocomposites. Cellulose 17:779–791. https://doi.org/10.1007/s10570-010-9427-5

Ahvenainen P, Kontro I, Svedström K (2016) Comparison of sample crystallinity determination methods by X-ray diffraction for challenging cellulose I materials. Cellulose 23:1073–1086. https://doi.org/10.1007/s10570-016-0881-6

Berggren R, Molin U, Berthold F et al (2002) Alkaline degradation of birch and spruce: influence of degradation conditions on molecular mass distributions and fibre strength. Carbohydr Polym 51:255–264. https://doi.org/10.1016/S0144-8617(02)00160-1

Binz A (1898) Die Mercerisation Der Baumwolle. Z für Angew Chemie 11:595–600. https://doi.org/10.1002/ange.18980112602

Bunsell AR, Harris B (1974) Hybrid carbon and glass fibre composites. Composites 5:157–164. https://doi.org/10.1016/0010-4361(74)90107-4

Daicho K, Saito T, Fujisawa S, Isogai A (2018) The crystallinity of nanocellulose: dispersion-induced disordering of the grain boundary in biologically structured cellulose. ACS Appl Nano Mater 1:5774–5785. https://doi.org/10.1021/acsanm.8b01438

Daicho K, Fujisawa S, Saito T (2022) Linear correlation between true density and crystallinity of regenerated and mercerized celluloses. Biomacromolecules. https://doi.org/10.1021/acs.biomac.2c01067

Djahedi C, Berglund LA, Wohlert J (2015) Molecular deformation mechanisms in cellulose allomorphs and the role of hydrogen bonds. Carbohydr Polym 130:175–182. https://doi.org/10.1016/j.carbpol.2015.04.073

Faria-Tischer PCS, Tischer CA, Heux L et al (2015) Preparation of cellulose II and IIII films by allomorphic conversion of bacterial cellulose I pellicles. Mater Sci Eng C 51:167–173. https://doi.org/10.1016/j.msec.2015.02.025

Fijoł N, Aguilar-Sánchez A, Ruiz-Caldas MX et al (2023) 3D printed polylactic acid (PLA) filters reinforced with polysaccharide nanofibers for metal ions capture and microplastics separation from water. Chem Eng J. https://doi.org/10.1016/j.cej.2022.141153

Fink HP, Weigel P, Purz HJ, Ganster J (2001) Structure formation of regenerated cellulose materials from NMMO-solutions. Prog Polym Sci 26:1473–1524. https://doi.org/10.1016/S0079-6700(01)00025-9

French AD (2014) Idealized powder diffraction patterns for cellulose polymorphs. Cellulose 21:885–896. https://doi.org/10.1007/s10570-013-0030-4

Fujisaki Y, Koga H, Nakajima Y et al (2014) Transparent nanopaper-based flexible organic thin-film transistor array. Adv Funct Mater 24:1657–1663. https://doi.org/10.1002/adfm.201303024

Fuller JD, Wisnom MR (2015) Pseudo-ductility and damage suppression in thin ply CFRP angle-ply laminates. Compos Part A Appl Sci Manuf 69:64–71. https://doi.org/10.1016/j.compositesa.2014.11.004

Gindl W, Keckes J (2005) All-cellulose nanocomposite. Polymer 46:10221–10225. https://doi.org/10.1016/j.polymer.2005.08.040

Goldthwait CF (1965) Shrinkage of cotton fibers in sodium hydroxide solutions and resulting elastic properties. Text Res J 35:986–992. https://doi.org/10.1177/004051756503501104

Guzman-Puyol S, Hierrezuelo J, Benítez JJ et al (2022) Transparent, UV-blocking, and high barrier cellulose-based bioplastics with naringin as active food packaging materials. Int J Biol Macromol 209:1985–1994. https://doi.org/10.1016/j.ijbiomac.2022.04.177

Guzman-Puyol S, Tedeschi G, Goldoni L et al (2022) Grease-proof, hydrophobic, and biodegradable food packaging bioplastics from C6-fluorinated cellulose esters. Food Hydrocoll. https://doi.org/10.1016/j.foodhyd.2022.107562

Hermans PH, Weidinger A (1949) X-ray studies on the crystallinity of cellulose. J Polym Sci 4:135–144. https://doi.org/10.1002/pol.1949.120040203

Hervy M, Santmarti A, Lahtinen P et al (2017) Sample geometry dependency on the measured tensile properties of cellulose nanopapers. Mater Des 121:421–429. https://doi.org/10.1016/j.matdes.2017.02.081

Hu G, Chen L, Zhao S, Hong FF (2022) Mercerization of tubular bacterial nanocellulose for control of the size and performance of small-caliber vascular grafts. Chem Eng J 428:131104. https://doi.org/10.1016/j.cej.2021.131104

Josset S, Orsolini P, Siqueira G et al (2014) Energy consumption of the nanofibrillation of bleached pulp, wheat straw and recycled newspaper through a grinding process. Nord Pulp Pap Res J 29:167–175. https://doi.org/10.3183/NPPRJ-2014-29-01-p167-175

Kim NH, Imai T, Wada M, Sugiyama J (2006) Molecular directionality in cellulose polymorphs. Biomacromol 7:274–280. https://doi.org/10.1021/bm0506391

Koga H, Saito T, Kitaoka T et al (2013) Transparent, conductive, and printable composites consisting of TEMPO-oxidized nanocellulose and carbon nanotube. Biomacromol 14:1160–1165. https://doi.org/10.1021/bm400075f

Koga H, Nogi M, Komoda N et al (2014) Uniformly connected conductive networks on cellulose nanofiber paper for transparent paper electronics. NPG Asia Mater 6:1–8. https://doi.org/10.1038/am.2014.9

Kolpak FJ, Weih M, Blackwell J (1978) Mercerization of cellulose: 1. Determination of the structure of Mercerized cotton. Polymer 19:123–131. https://doi.org/10.1016/0032-3861(78)90027-7

Koocheki A, Ghandi A, Razavi SMA et al (2009) The rheological properties of ketchup as a function of different hydrocolloids and temperature. Int J Food Sci Technol 44:596–602. https://doi.org/10.1111/j.1365-2621.2008.01868.x

Kriechbaum K, Bergström L (2020) Antioxidant and UV-Blocking leather-inspired nanocellulose-based films with High Wet Strength. Biomacromol 21:1720–1728. https://doi.org/10.1021/acs.biomac.9b01655

Kroon-Batenburg LMJ, Kroon J (1997) The crystal and molecular structures of cellulose I and II. Glycoconj J 14:677–690. https://doi.org/10.1023/A:1018509231331

Leppänen I, Vikman M, Harlin A, Orelma H (2020) Enzymatic degradation and pilot-scale composting of cellulose-based films with different Chemical structures. J Polym Environ 28:458–470. https://doi.org/10.1007/s10924-019-01621-w

Mautner A (2020) Nanocellulose water treatment membranes and filters: a review. Polym Int 69:741–751. https://doi.org/10.1002/pi.5993

Mautner A, Lee K-Y, Tammelin T et al (2015) Cellulose nanopapers as tight aqueous ultra-filtration membranes. React Funct Polym 86:209–214. https://doi.org/10.1016/j.reactfunctpolym.2014.09.014

Mautner A, Maples HA, Sehaqui H et al (2016) Nitrate removal from water using a nanopaper ion-exchanger. Environ Sci Water Res Technol 2:117–124. https://doi.org/10.1039/c5ew00139k

Mautner A, Lucenius J, Österberg M, Bismarck A (2017) Multilayer nanopaper based composites. Cellulose 24:1759–1773. https://doi.org/10.1007/s10570-017-1220-2

Mautner A, Mayer F, Hervy M et al (2018) Better together: synergy in nanocellulose blends. Philos Trans R Soc A Math Phys Eng Sci 376:20170043. https://doi.org/10.1098/rsta.2017.0043

Mautner A, Kobkeatthawin T, Mayer F et al (2019) Rapid water softening with TEMPO-oxidized/phosphorylated nanopapers. Nanomaterials 9:1–18. https://doi.org/10.3390/nano9020136

Mautner A, Nawawi WMFW, Lee KY, Bismarck A (2020) High porosity cellulose nanopapers as reinforcement in multi-layer epoxy laminates. Compos Part A Appl Sci Manuf 131:105779. https://doi.org/10.1016/j.compositesa.2020.105779

Moon RJ, Martini A, Nairn J et al (2011) Cellulose nanomaterials review: structure, properties and nanocomposites. Chem Soc Rev 40:3941. https://doi.org/10.1039/c0cs00108b

Nishino T, Takano K, Nakamae K (1995) Elastic modulus of the crystalline regions of cellulose polymorphs. J Polym Sci Part B Polym Phys 33:1647–1651. https://doi.org/10.1002/polb.1995.090331110

Nishiyama Y, Langan P, Chanzy H (2002) Crystal structure and hydrogen-bonding system in cellulose I_β from synchrotron X-ray and neutron fiber diffraction. J Am Chem Soc 124:9074–9082. https://doi.org/10.1021/ja0257319

Nishiyama Y, Sugiyama J, Chanzy H, Langan P (2003) Crystal structure and hydrogen bonding system in cellulose I α from synchrotron x-ray and neutron fiber diffraction. J Am Chem Soc 125:14300–14306. https://doi.org/10.1021/ja037055w

Sawada D, Nishiyama Y, Shah R et al (2022) Untangling the threads of cellulose mercerization. Nat Commun 13:1–6. https://doi.org/10.1038/s41467-022-33812-w

Sehaqui H, Zhou Q, Ikkala O, Berglund LA (2011) Strong and tough cellulose nanopaper with high specific surface area and porosity. Biomacromol 12:3638–3644. https://doi.org/10.1021/bm2008907

Walther A, Lossada F, Benselfelt T et al (2020) Best practice for reporting wet mechanical properties of nanocellulose-based materials. Biomacromol 21:2536–2540. https://doi.org/10.1021/acs.biomac.0c00330

Wang H, Li D, Yano H, Abe K (2014) Preparation of tough cellulose II nanofibers with high thermal stability from wood. Cellulose 21:1505–1515. https://doi.org/10.1007/s10570-014-0222-6

Wloch D, Herrera N, Lee KY (2023) Optically transparent laminated acrylic composites reinforced with mercerised bacterial cellulose nanopaper. Compos Part A Appl Sci Manuf 172:107583. https://doi.org/10.1016/j.compositesa.2023.107583

Xu X, Zhou J, Jiang L et al (2016) Highly transparent, low-haze, hybrid cellulose nanopaper as electrodes for flexible electronics. Nanoscale 8:12294–12306. https://doi.org/10.1039/c6nr02245f

Zhu H, Fang Z, Preston C et al (2014) Transparent paper: fabrications, properties, and device applications. Energy Environ Sci 7:269–287. https://doi.org/10.1039/C3EE43024C